Front. Phys. 11(6), 114206 (2016)
DOI 10.1007/s11467-016-0589-y

RESEARCH ARTICLE

Perfect digital holographic imaging with high resolution using a submillimeter-dimension CCD sensor

Hua-Ying Wang (王华英)[1], **Nan-Yan Xiong** (熊南燕)[2], **Jun-Xiang Li** (栗军香)[3], **Zhao Dong** (董昭)[1], **Xia-Nan Jiang** (江夏男)[1], **Feng Fan** (范锋)[1], **Ya-Guang Geng** (耿亚光)[4], **Qiao-Fen Zhu** (朱巧芬)[1,†]

[1] *College of Science, Hebei University of Engineering, Handan 056038, China*
[2] *College of Medicine, Hebei University of Engineering, Handan 056038, China*
[3] *College of Clinical Medicine, Hebei University of Engineering, Handan 056038, China*
[4] *Hebei Hanguang Industry Company Limited, Handan 056028, China*
Corresponding author. E-mail: [†] *zqf800404@163.com*
Received August 6, 2015; accepted February 16, 2016

In order to improve the resolution of digital holography with a common-dimension charge-coupled device (CCD) sensor, the point spread functions are briefly derived for the commonly used and practical post-magnification, pre-magnification, and image-plane digital holographic microscopic systems. The ultimate resolutions of these systems are analyzed and compared. The results show that the ultimate lateral resolution of pre-magnification digital holography is superior to that of post-magnification digital holography in the same conditions. We also demonstrate that the ultimate lateral resolution of image-plane digital holography has no correlation with the photosensitive dimension of the CCD sensor, and it is not significantly related to the pixel size of the sensor. Moreover, both the ultimate resolution and the imaging quality of image-plane digital holography are superior to that of pre- and post-magnification digital holographic microscopy. High-resolution imaging, whose resolution is close to the ultimate resolution of the microscope objective, can be achieved by image-plane digital holography even with a submillimeter-dimension sensor. This system, by which perfect imaging can be achieved, is optimal for commonly used digital holographic microscopy. Experimental results demonstrate the correctness of the theoretical analysis.

Keywords digital holography, digital holographic microscopy, image-plane digital holography, ultimate lateral resolution, small-dimension CCD

PACS numbers 42.30.Kq, 42.40.Kw, 42.30.-d

1 Introduction

Digital holographic microscopy (DHM) has been established as a very powerful microscopic imaging and measurement tool [1] that possesses real-time, non-contact, non-invasive, high-sensitivity features. Moreover, DHM offers significant advantages over conventional microscopy in accessibility to quantitative amplitude and phase information, and in flexible digital processing such as storage, filtering, auto-focusing, aberration compensation, and display. DHM has been widely used in many fields such as biomedical science [2–7], micro- and nano-fabrication [8–10], materials science [11–13], the particle field [14–17], atomic physics [18], and the thermal energy field [19]. Nevertheless, the resolution and image quality of the most commonly used pre-magnification digital holographic microscopy (Pre-MDHM) and post-magnification digital holographic microscopy (Post-MDHM) are restricted by the photosensitive dimensions and the pixel size of the sensor, which has greatly limited the application of DHM. To improve the resolution and image quality of DHM, many approaches have recently been proposed, such as structured light illumination [20, 21], synthetic aperture [22–24], super-resolution [17, 25], interferometric microscopy [26], and vortex light illumination [27]. These methods can improve the resolution theoretically; however, so far, the improvement has not been achieved in microscopic imaging. In addition, these methods make the holographic recording system more complicated and the reconstruction slower. We find that image-plane digital holographic

Frontiers of Physics

microscopy (IPDHM) has many unique advantages over other kinds of DHM, such as a low-coherent source and very simple and quick numerical reconstruction. Another important advantage is that the resolution is independent of the photosensitive dimensions of the recording device and is consistent for each point of the image plane, which makes high resolution and high-quality imaging achievable by using only a CCD sensor with very small dimensions. Recently, Sánchez-Ortiga *et al.* proposed a special DHM system formed by an infinity-corrected microscopic objective (MO) and a tube lens (TL) in the object path [28], which has better performance than that of the most commonly used DHM, especially in accurate phase imaging. In this paper, however, we discuss only the conventional DHM system.

The remainder of this paper is organized as follows. In Section 2, the point spread function (PSF) of practical Post-MDHM and IPDHM is briefly derived based on scalar diffraction theory. Then, the ultimate lateral resolutions (ULRs) of these systems are analyzed and compared. Some experimental results are presented in Section 3 to demonstrate the correctness of the analysis. Finally, Section 4 summarizes the main conclusions of this paper.

2 Theoretical analysis

2.1 Recording and reconstruction of digital hologram

The setup of off-axis DHM recorded with a plane reference wave is shown in Fig. 1. The light from the laser source is divided by PBS into two beams with different polarization directions. The half-wave plate between the light source and PBS adjusts the intensity of the two beams. Then, the two beams are expanded and collimated by BE_1 and BE_2, respectively, to become two plane waves. One of the beams is the reference wave, and the other illuminates the sample. The object is pre-

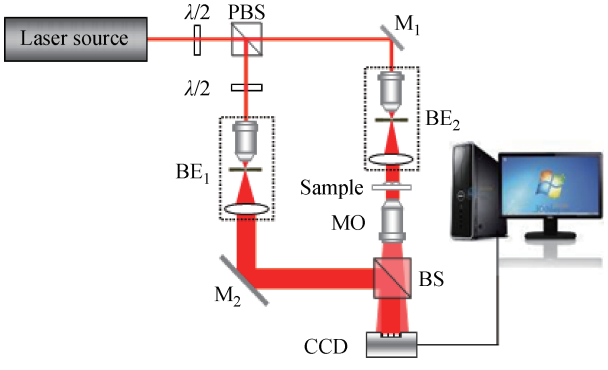

Fig. 1 The schematic of the setup of off-axis DHM recorded with plane reference wave.

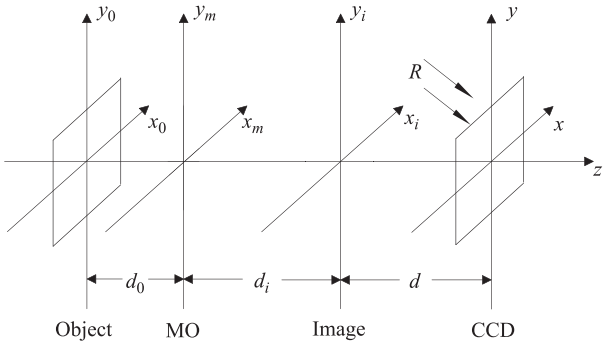

Fig. 2 The coordinate schematic of off-axis Post-MDHM system recorded with planar reference wave.

magnified and imaged by an MO. The digital hologram formed by interference between the object and reference waves is recorded by a CCD sensor and stored on a frame grab card in the computer. In the reference wave path, another half-wave plate produces the same polarization states of the two waves on the CCD plane. In Fig. 1, the plane reference wave will become a spherical wave by inserting an MO in the reference beam.

Figure 2 depicts the coordinate schematic of off-axis Post-MDHM recorded with the plane reference wave, where MO is represented by a positive lens whose focal length is f. The object plane, MO plane, image plane, and CCD plane are located at $x_0 - y_0, x_m - y_m, x_i - y_i$, and $x - y$, respectively. The optical axis z of the MO perpendicularly passes through the center of the four planes. The objective distance and the image distance of the MO are represented by d_0 and d_i, respectively. The hologram recording distance is d, and R is the plane reference wave. In Fig. 2, if the CCD sensor is located in front of the image plane, the system becomes Pre-MDHM; and if the recording plane coincides with the image plane, which means$d = 0$, the DHM becomes IPDHM.

According to the paraxial Fresnel diffraction integral and the Fourier transform properties of lenses, the complex amplitude distribution of the object wave field at the CCD plane is given by [29]

$$O(x,y) = \frac{\exp[\mathrm{i}k(d_i+d)]}{\mathrm{i}\lambda(d_i+d)} \int_{-\infty}^{\infty}\int_{-\infty}^{\infty} U(x_m,y_m) \times \mathrm{circ}\left(\frac{\sqrt{x_m^2+y_m^2}}{D/2}\right) \exp\left[-\frac{\mathrm{i}k}{2f}(x_m^2+y_m^2)\right] \times \exp\left\{\frac{\mathrm{i}k}{2(d_i+d)}[(x-x_m)^2+(y-y_m)^2]\right\} \mathrm{d}x_m \mathrm{d}y_m, \quad (1)$$

where λ is the wavelength of the illumination light, $\mathrm{i} = \sqrt{-1}, k = 2\pi/\lambda$ is the wavenumber, D is the aperture diameter of the MO, and $\otimes$ refers to the convolution

operation. The complex amplitude distribution of the object wave in the front surface of the MO is $U(x_m, y_m)$ and is written as

$$U(x_m,y_m)=\frac{\exp(\mathrm{i}kd_0)}{\mathrm{i}\lambda d_0}\int_{-\infty}^{\infty}\int_{-\infty}^{\infty}o(x_0,y_0)\times\exp\left\{\frac{\mathrm{i}k}{2d_0}[(x_m-x_0)^2+(y_m-y_0)^2]\right\}\mathrm{d}x_0\mathrm{d}y_0, \tag{2}$$

where $o(x_0, y_0)$ is the complex amplitude transmittance of the object.

The interference intensity in the recording plane is given by

$$H(x,y)=|O(x,y)|^2+|R(x,y)|^2+R^*(x,y)O(x,y)+O^*(x,y)R(x,y), \tag{3}$$

where * represents the complex conjugate. As shown in Fig. 2, $R(x, y)$ is the complex amplitude of the plane reference wave field and is found by

$$R(x,y)=R_0\exp[-\mathrm{i}2\pi(f_x x+f_y y)], \tag{4}$$

where fx and fy are the spatial frequency components in the two perpendicular directions.

Assume that $\Delta x, \Delta y$ is the pixel size and N_x, N_y represents the pixel numbers of the CCD in two perpendicular directions, and $\alpha, \beta (0 < \alpha, \beta \leq 1)$, which is usually very close to one, represents the fill factors of the CCD sensor. Taking into account the discretization and the pixel averaging effect of the CCD sensor, the recorded digital hologram is written as [1]

$$H_D(x,y)=\left[H(x,y)\otimes\mathrm{rect}\left(\frac{x}{\alpha\Delta x},\frac{y}{\beta\Delta y}\right)\right]\times\mathrm{comb}\left(\frac{x}{\Delta x},\frac{y}{\Delta y}\right)\mathrm{rect}\left(\frac{x}{N_x\Delta x},\frac{y}{N_y\Delta y}\right). \tag{5}$$

The reconstruction of digital holography is achieved by numerically simulating the diffraction process of the optical wave field. However, for simplicity, the following analysis is still based on the continuous form of the optical wave field. In Post-MDHM, because the final image plane is in front of the hologram plane, the image field is calculated by back-propagating the hologram information to the image plane. By applying the frequency domain filtering method to eliminate the zero-order and undesired −1 order terms, the +1 order diffraction wave field of the hologram can be obtained,

$$U_{+1}(x,y)=\mathrm{FT}^{-1}\{\mathrm{FT}\,[H_D(x,y)]\cdot W_{+1}(f_x,f_y)\}, \tag{6}$$

where $W_{+1}(f_x, f_y)$ is the transparent filtering window function, which is transparent for the +1 order spectrum. The window should be selected not only so that it contains as much high-frequency information as possible but also so that the +1 order spectrum avoids interference by the zero-order term. According to the angular spectrum formula of scalar diffraction and the linear system theory, the complex amplitude of the reconstructed image field is obtained by

$$U(x_i,y_i)=\mathrm{FT}^{-1}\{\mathrm{FT}\,\{R(x,y)U_{+1}(x,y)\}G(f_x,f_y)\} \tag{7}$$

and

$$G(f_x,f_y)=\exp\left\{-\mathrm{i}kd\sqrt{1-(\lambda f_x)^2-(\lambda f_y)^2}\right\}, \tag{8}$$

where FT and FT^{-1} denote two-dimensional forward and inverse Fourier transform, respectively, and $G(f_x, f_y)$ is the transfer function of light propagation in free space. The difference between Pre-MDHM and Post-MDHM in the reconstruction process is the opposite propagating direction of the optical wave field from the hologram plane to image plane, which means that the image field of Pre-MDHM can be determined by replacing d with $-d$ in Eq. (8).

Because the CCD plane is coincident with the image plane, the hologram recording distance d is zero in IPDHM. Thus, with $d = 0$ in Eq. (1), the complex amplitude distribution of the object wave field at the CCD plane can be obtained. For hologram reconstruction of IPDHM, the collimated plane wave is usually used as the reconstructing reference wave. Because there is no diffraction from the hologram plane to the image plane, which leads to $G(f_x, f_y) = 1$, the process of numerical reconstruction is much simpler. The complex amplitude of the reconstructed original image wave field is

$$U(x_i,y_i)=\mathrm{FT}^{-1}\{\mathrm{FT}\,[H_D(x,y)]\cdot W_{+1}(f_x,f_y)\}. \tag{9}$$

From Eq. (9), one can see that if a proper filtering window is applied so that the +1 order term is completely selected out, the filtered hologram itself is the amplitude distribution of the reconstructed image wave field. Therefore, the recording of a high-quality digital hologram is of crucial importance [28].

2.2 Ultimate lateral resolution of the DHM system

The ultimate lateral resolution (ULR) of an imaging system depends on the main lobe width of the amplitude PSF of the system. To obtain the PSF of a holographic system, it is supposed that a point object with unit intensity is located at (ξ, η) in the $x_0 - y_0$ plane and is represented by $\delta(x_0 - \xi, y_0 - \eta)$. Substituting $o(x_0, y_0)$ with $\delta(x_0 - \xi, y_0 - \eta)$ into Eq. (2), the amplitude distribution of the spherical wave field on the MO plane

formed by the point source can be obtained, and it is

$$U(x_m, y_m) = \frac{\exp(\mathrm{i}kd_0)}{\mathrm{i}\lambda d_0} \times \exp\left\{\frac{\mathrm{i}k}{2d_0}[(x_m-\xi)^2 + (y_m-\eta)^2]\right\}. \quad (10)$$

To obtain the PSF of the Post-MDHM system, we use the Fresnel diffraction formula for reconstructing the hologram and take into account the finite aperture of the CCD but ignore the sampling and averaging effect of CCD pixels in Eq. (5). By combining Eqs. (1) and (3)–(5) with Eq. (10), the PSF of the Post-MDHM system, whose detailed derivation process is very similar to that of Ref. [29], is as follows:

$$\begin{aligned} &PSF_{+1}(x_i, y_i) \\ &= C\exp\left[-\frac{\mathrm{i}\pi}{\lambda d}(x_i^2 + y_i^2)\right] \\ &\quad \times \exp\left[\frac{\mathrm{i}\pi}{\lambda d_0}\left(1 + \frac{d_i + d}{dd_0}d_i\right)(\xi^2 + \eta^2)\right] \times \left\{\frac{J_1[\pi D\rho]}{\rho}\right. \\ &\quad \otimes\left\{\mathrm{sinc}\left[\frac{N_x\Delta x}{\lambda d}(x_i + M\xi)\right]\mathrm{sinc}\left[\frac{N_y\Delta y}{\lambda d}(y_i + M\eta)\right]\right. \\ &\quad \left.\left. \times \exp\left[-\frac{\mathrm{i}\pi(d_i + d)}{\lambda dd_i}(x_i^2 + y_i^2)\right]\right\}\right\}, \end{aligned} \quad (11)$$

where

$$\rho = \sqrt{(x_i + M\xi)^2 + (y_i + M\eta)^2}/(\lambda d_i) \quad (12)$$

and C is real constants. The definition of the sinc{} function is $\mathrm{sinc}\,(x) = \sin(\pi x)/\pi x$, and $M = d_i/d_0$ is the magnification of the reconstructed image. Moreover, the most common case in which the square pixel and equal pixel number in the perpendicular directions and the object-image relation $1/d_0 + 1/d_i = 1/f$ has also been used. For the Pre-MDHM system, the same expression as Eq. (11) is used except d is replaced with $-d$ in all the exponential functions.

From Eq. (11), one can see that the Post- and Pre-MDHM systems are cascade imaging systems, in which the amplitude distributions of the PSFs of the CCD and MO imaging units are $\mathrm{sinc}\,[Nx\Delta x/(\lambda d)(x_i + M\xi)]\mathrm{sinc}\,[Ny\Delta y/(\lambda d)(y_i + M\eta)]$ and $J_1[\pi D\rho]/\rho$, respectively. According to the Rayleigh criterion, the lateral resolution of an imaging system equals the half-width of the amplitude PSF. Thus, the theoretical ULRs of the two imaging units, which means the distance between the closest two points resolved by the imaging system in the object plane, are $\delta_{\mathrm{CCD}} = \max\{\lambda d/(MNx\Delta x), \lambda d/(MNy\Delta y)\}$ and $\delta_{\mathrm{MO}} = 0.61\lambda/\mathrm{NA}$, respectively. Because the convolution operation has a broadening effect, the ULRs of Pre- and Post-MDHM systems are inferior to those of CCD and MO imaging units. Evidently, one can improve the resolution by choosing a large numerical aperture (NA), large magnification of the MO, and large CCD sensor dimensions, but this improvement is very restricted to the parameters. Furthermore, when other parameters remain unchanged, the smaller the hologram recording distance d, the higher is the ULR of the DHM system. The limiting case of both Pre- and Post-MDHM is the hologram distance $d = 0$, in which the system is only IPDHM. Thus, by inference, the IPDHM system has the highest imaging resolution compared to the other two commonly used DHMs.

Although Pre-MDHM and Post-MDHM have very similar expressions, the ULR of Post-MDHM is inferior to that of Pre-MDHM in the same conditions because less high-frequency information is in the hologram recorded by Post-MDHM. To illustrate this point, a schematic diagram of the microscopic imaging system is given in Fig. 3. If we suppose that the imaging system is perfect, the B'A' is the magnified replication of AB. If a reference wave is introduced to the image system, holographic imaging is achieved. When a CCD sensor is placed at the image plane, in front of and behind the image plane, such as B'A', DE, and FG, as shown in Fig. 3, the digital holograms are recorded by IPDHM, Pre-MDHM, and Post-MDHM, respectively. Since the dimensions of the CCD sensor are limited, which is L_x = B'C' in Fig. 3, the object spatial frequency information encoded in different holograms is different. From Fig. 3, one can see that the high-frequency information recorded by Post-MDHM is less than that of both IPDHM and Pre-MDHM.

Theoretically, the +1 order diffraction term can be exactly obtained. In this case, Eq. (9) becomes

$$U_{+1}(x_i, y_i) = \left[R^*(x, y)O(x, y) \otimes \mathrm{rect}\left(\frac{x}{\alpha\Delta x}, \frac{y}{\beta\Delta y}\right)\right] \times \mathrm{comb}\left(\frac{x}{\Delta x}, \frac{y}{\Delta y}\right)\mathrm{rect}\left(\frac{x}{N_x\Delta x}, \frac{y}{N_y\Delta y}\right). \quad (13)$$

By combining Eq. (1), (4), and (10) with (13) and by some mathematical deduction, the PSF of the original image field obtained by IPDHM is

$$\begin{aligned} &PSF_{+1}(x_i, y_i) \\ &= C'\exp\left[\frac{\mathrm{i}k}{2d_0}(\xi^2 + \eta^2)\right] \times \left\{\left\{\exp\left[\frac{\mathrm{i}k}{2d_i}(x_i^2 + y_i^2)\right]\right.\right. \\ &\quad \left.\times \exp[\mathrm{i}2\pi(f_x x_i + f_y y_i)]\frac{J_1[\pi D\rho]}{\rho}\right\} \\ &\quad \otimes\mathrm{rect}\left(\frac{x_i}{\alpha\Delta x}, \frac{y_i}{\beta\Delta y}\right)\Big\}\mathrm{comb}\left(\frac{x_i}{\Delta x}, \frac{y_i}{\Delta y}\right) \\ &\quad \times\mathrm{rect}\left(\frac{x_i}{N_x\Delta x}, \frac{y_i}{N_y\Delta y}\right). \end{aligned} \quad (14)$$

The pixel averaging and sampling effect have been taken into account in Eq. (14). For the case of a spherical refer-

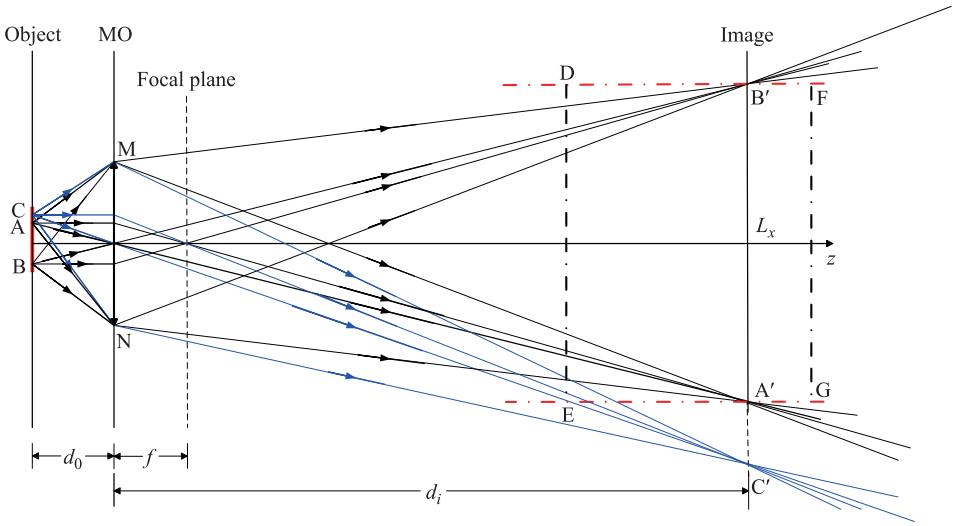

Fig. 3 The schematic for MO imaging and for recording magnified image of CCD.

ence wave, the PSF has the same form as Eq. (14) except for the different exponential function.

In Eq. (14), the ULR of the MO imaging unit is still given by $J_1[\pi D\rho]/\rho$. The function rect $(x_i/Nx\Delta x, y_i/Ny\Delta y)$ together with the magnification M determines the field of view (FOV). The function comb $(x_i/\Delta x, y_i/\Delta y)$ describes the sampling process in the image plane but has no correlation with the system resolution because of the large imaging magnification and the smaller pixel size of the commonly used CCD in microscopic imaging. The effect of the convolution operation with the function rect $(x_i/\alpha\Delta x, y_i/\beta\Delta y)$ is smoothing the sharpness of the function $J_1[\pi D\rho]/\rho$. Due to the relatively small size of $\alpha\Delta y$ and $\beta\Delta y$, the blurring effect is very small, which means that the convolution operations can deteriorate the resolution slightly. There is the same convolution operation in all kinds of digital holography. Moreover, it is evident that the ULR of IPDHM has nothing to do with the dimensions of the sensor. Therefore, it is concluded that the ULR of IPDHM depends mainly on the NA of the MO used and the wavelength of the laser. The parameters of the recording sensor have little effect on the ULR, which is very different from other kinds of digital holography.

If the pixel averaging and sampling effect are ignored, Eq. (14) becomes

$$\begin{aligned} &PSF_{+1}(x_i, y_i) \\ &= C'' \exp\left[\frac{\mathrm{i}k}{2d_0}(\xi^2+\eta^2)\right]\left\{\exp\left[\frac{\mathrm{i}k}{2d_i}(x_i^2+y_i^2)\right]\right. \\ &\quad \left.\times \exp[\mathrm{i}2\pi(f_x x_i + f_y y_i)]\,\frac{J_1[\pi D\rho]}{\rho}\right\} \\ &\quad \times \mathrm{rect}\left(\frac{x_i}{N_x\Delta x}, \frac{y_i}{N_y\Delta y}\right). \end{aligned} \tag{15}$$

2.3 Advantages of IPDHM

There are many advantages of IPDHM compared to Pre- and Post-MDHM. Apart from those mentioned earlier, there are three main kinds of advantages to be analyzed.

(i) High-resolution imaging can be achieved by using a CCD sensor with very small dimensions.

Since the ULR of an IPDHM system does not depend on the sensor dimensions, high resolution can be achieved by exploring a CCD sensor with very small dimensions, which can greatly reduce the cost of the DHM system. This is not applicable for other kinds of digital holography.

(ii) The imaging quality of IPDHM is much better than that of Pre- and Post-MDHM.

The high-performance imaging of IPDHM is mainly reflected in a number of aspects. First, its imaging resolution is superior to that of Pre- or Post-MDHM, as mentioned above. Second, the resolution of the intensity image of every point in the FOV is the same, which can be explained by Eq. (14). From Eq. (14), it is evident that the amplitude distribution of PSF is irrelevant to the coordinates of the object point except for the term $J_1[\pi D\rho]/\rho$, thus, the ULR is also irrelevant to the coordinates of the object point. Third, its imaging is perfect. This is because the image plane is a very special plane in which the CCD sensor can receive all the frequency components emitted from any point in the range of FOV and passed through the MO. However, for Pre- and Post-MDHM, some high-frequency components emitted from the edge of FOV and passed through the MO cannot be received by the CCD sensor. The larger the recording distance, the greater the loss of information, which means that the imaging resolution of the marginal area imaged by Pre- and Post-MDHM is inferior to that of the center

area. Thus, the imaging of Pre- and Post-MDHM is imperfect. Fourth, it is very important to obtain the recording distance accurately in digital holography, which influences the phase measurement accuracy dramatically. Because the recording distance of the image-plane hologram is zero, phase error is not introduced by recording distance error. Therefore, the phase error reconstructed by IPDHM is smaller than that of other kinds of digital holography.

(iii) Imaging with large FOV can be easily achieved by IPDHM.

In DHM, the FOV depends mainly on the parameters of the MO used. To increase the FOV, the image fusion method is usually adopted by recording multiple holograms. This is very complicated for Pre- and Post-MDHM because the object information carried by each point of the hologram is associated with each other. However, for IPDHM, because the object information carried by different points of the hologram is not related to each other, the fusion of holograms is very easy. On the other hand, the image reconstructed by IPDHM possesses the same quality and resolution at the center as at the edge of the FOV, which makes the fusion of the reconstructed images also very easy. Moreover, because the recording device is located at the image plane, the recording process is very easy to control. In addition, high-quality imaging can be achieved by using a low-cost recording device.

Owing to the effects of the quadratic phase introduced by the MO, which results in the shift-variant nature of the regular DHM system, there are different phase errors at different positions in the reconstructed phase images [28]. According to Ref. [28], the ruining effects can be eliminated by introducing an infinity-corrected MO and a TL system in the object path so that a three-dimensional reconstructed image with small phase error can be obtained. Therefore, the above analyses are only applicable to the regular DHM. Taking into account the view that the quadratic phase also has unwanted effects in the digital hologram recording conditions to achieve diffraction-limited DHM [28], the aforementioned special DHM system generally performs better than the regular DHM system for phase imaging.

3 Experimental results

The experimental setup is shown in Fig. 1, in which the light source was a He-Ne laser with a 632.8 nm wavelength. The chosen sensor was a 1392 × 1032 pixel CCD with pixel size 4.65 μm × 4.65 μm and 16-bit gray level. We chose a 40x/0.65 MO for which NA/M = 0.016 and the focal length f = 4.65 mm. The theoretical ULR of the MO was 0.594 μm. In all the following experiments, the magnifications of the MO were adjusted to 40.0.

A negative 1951 USAF resolution target was placed in the near front of the MO focal plane, as shown in Fig. 1. Figure 4(a) is an original hologram with 1024 × 1024 pixels. By applying the adjacent pixel average with 2 × 2 to Fig. 4(a), a new hologram with pixel size 9.30 μm × 9.30 μm and 512 × 512 pixels was obtained, as shown in Fig. 4(e). The corresponding frequency spectra are presented in Figs. 4(b) and (f), in which the red rectangular areas are the filtered spectra used to reconstruct the original images. From Figs. 4(b) and (f), one can see that the size of the +1 order frequency spectrum almost achieved maximum to limit the loss of the high-frequency spectrum information as much as possi-

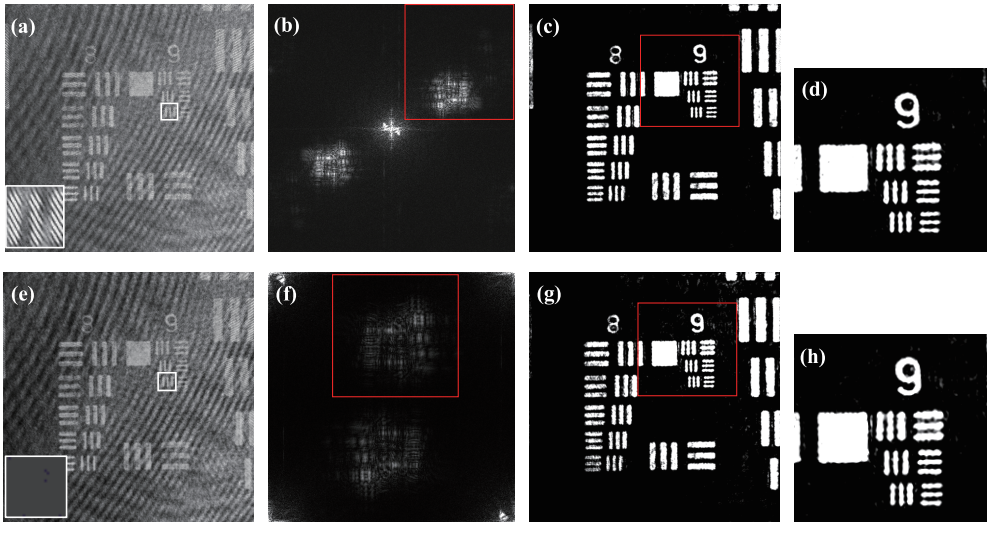

Fig. 4 The holograms (left columns) recorded with plane reference, frequency spectral (second columns), reconstructed intensity images (third columns), magnified images within the red rectangle (fourth columns). **(a–d)** pixel size 4.65 μm × 4.65 μm, **(e–h)** pixel size 9.30 μm × 9.30 μm.

ble. For simplicity, the same operation is applied to the following experimental results. The reconstructed intensity images of the two holograms are given in Figs. 4(c) and (g). Figures 4(d) and (h) are the magnified images in the red rectangle of Figs. 4(c) and (g), respectively, from which three elements of group 9 of the test target are clearly resolved. Note that the zero-order spectra were moved to the four corners in Fig. 4(f) to avoid overlapping the two first-order spectra and to obtain an entire first-order spectrum. By comparing Figs. 4(d) and (e), one can see that there is no apparent difference between them, which means that the lateral resolution of IPDHM depends very little on the pixel size of the sensor.

Figures 5(a), (d), and (g) are the tailored holograms from Fig. 4(a) with 512 × 512, 256 × 256, and 128 × 128 pixels, respectively. Figures 5(b), (e), and (h) are frequency spectra of the three holograms, and Figs. 5(c), (f), and (i) are the reconstructed intensity images. In Fig. 5(a), the three lines within the white rectangle are the three elements of group 9 of the test target, and its width is 0.78 μm, which is larger than the resolvable width of the system. By comparing the three intensity images, it is evident that the clarity of the lines does not degrade as the hologram size decreases, which demonstrates that the ULR has no correlation with the CCD sensor dimensions. The hologram size of Fig. 5(g) is just 0.595 mm.

To demonstrate the high performance of IPDHM with very small sensor dimensions for phase imaging, an experiment using human blood cells was conducted, and the results are shown in Figs. 6 and 7. Figures 6(a) and (b) are the original hologram recorded with a spherical reference wave and its frequency spectrum, respectively. The two- and three-dimensional phase images calculated with Eq. (9) are shown in Figs. 6(c) and (d), respectively, and Fig. 6(e) is the magnified image of the cell in the red ring of Fig. 6(c). Both Figs. 7(a) and (e) are tailored holograms from Fig. 6(a). By comparing Fig. 6

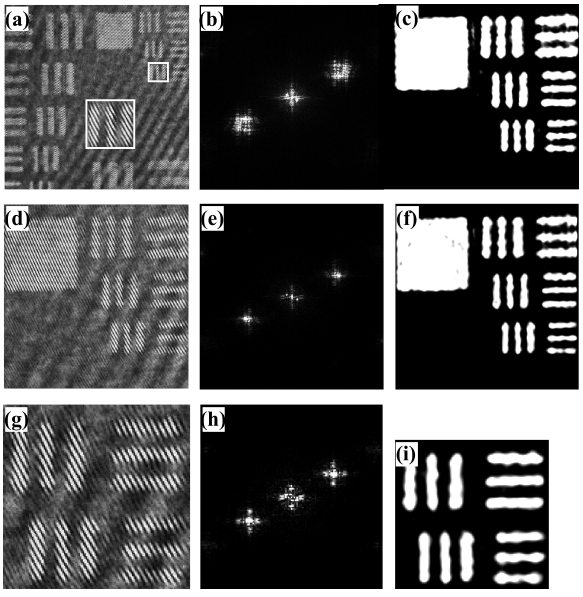

Fig. 5 The holograms (left columns) recorded with plane reference wave, frequency spectral (middle columns) and reconstructed intensity images (right columns). **(a–c)** 512×512, **(d–f)** 256 × 256, **(g–i)** 128 × 128.

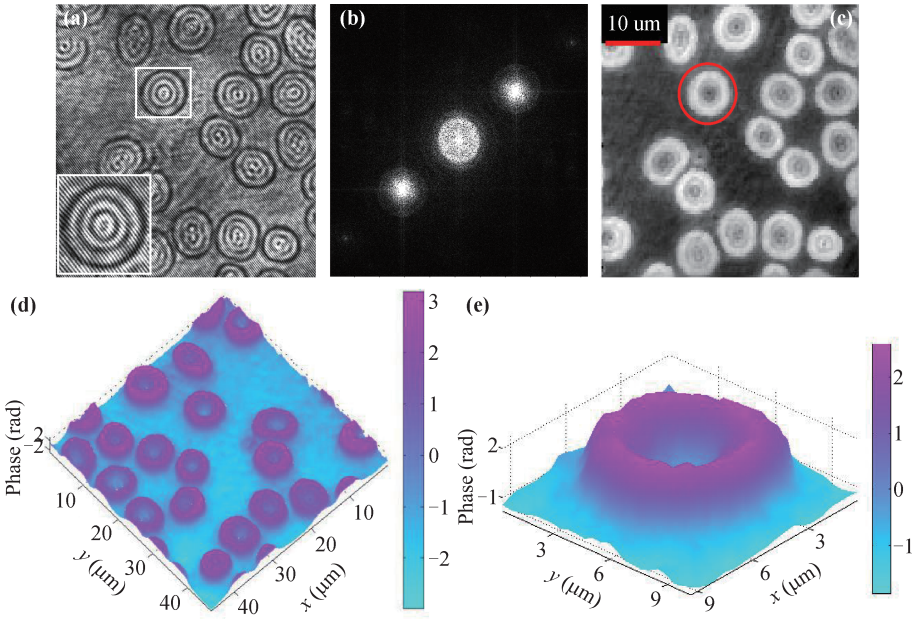

Fig. 6 The experimental results for human blood cell. **(a)** hologram (512 × 512), **(b)** frequency spectrum, **(c)** two-dimensional phase, **(d)** three-dimensional display of (c), **(e)** magnified image of the cell in the red ring of (c).

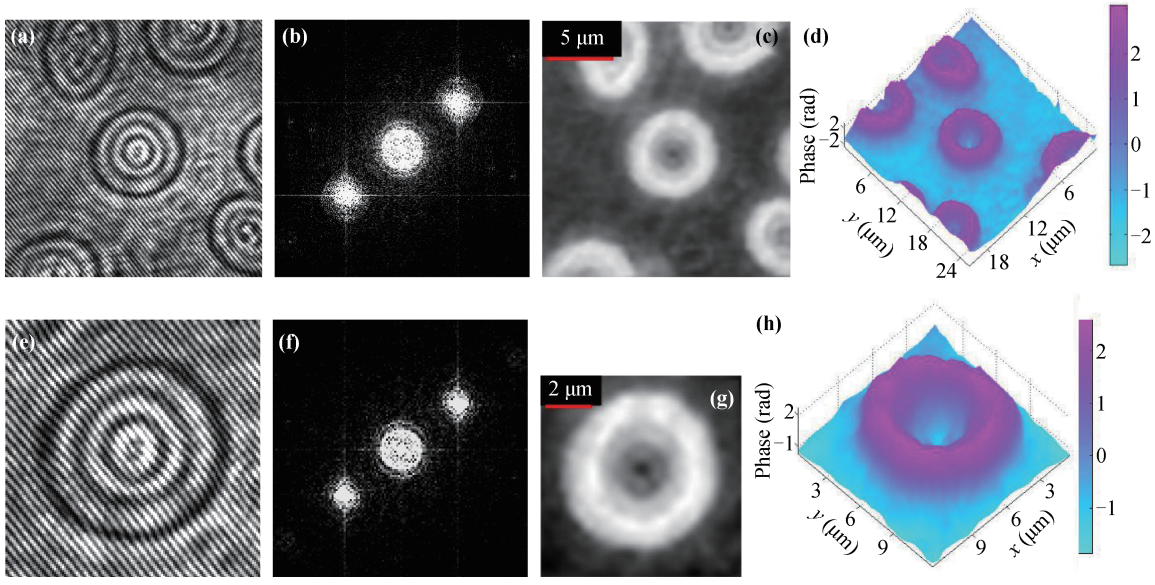

Fig. 7 The holograms tailored from Fig. 6(a) (left columns), the frequency spectral (second columns), the 2D reconstructed phase image and 3D display of the reconstructed phase (right columns). **(a–d)** 256 × 256, **(e–h)** 128 × 128.

with 7, it is obvious that high-resolution phase imaging was also achieved by IPDHM and by using a sensor with very small dimensions.

Figure 8(a) is an original hologram recorded by Post-MDHM with recording distance $d = 46$ mm and pixel number 1024×1024. In the experiment, the MO was the same as the one used in IPDHM. Figure 8(d) is the center part of Fig. 8(a) with pixel number 512×512. Figure 8(g) is the tailored hologram with pixel number 256×256 and from the top-right of Fig. 8(a). The middle column images are the frequency spectra of the three holograms, and the right column shows the corresponding intensity images. It is evident that the clarity of Figs. 8(f) and (i) is inferior to that of Fig. 8(c), which demonstrates that the ULR of Post-MDHM dramatically decreases with decreasing sensor size. Moreover, the edge of Fig. 8(f) is very blurry and dark, which demonstrates that part of the high-frequency spectra emitted from the edge area of the FOV and passed through the MO were lost in the recording process.

Figure 9 shows the experimental result obtained by Pre-MDHM in the same condition as for Fig. 8. Some high-frequency components of the FOV edge area were also lost in this case. A comparison of Fig. 9 with Fig. 8 shows that the lateral resolution of Pre-MDHM is higher than that of Post-MDHM.

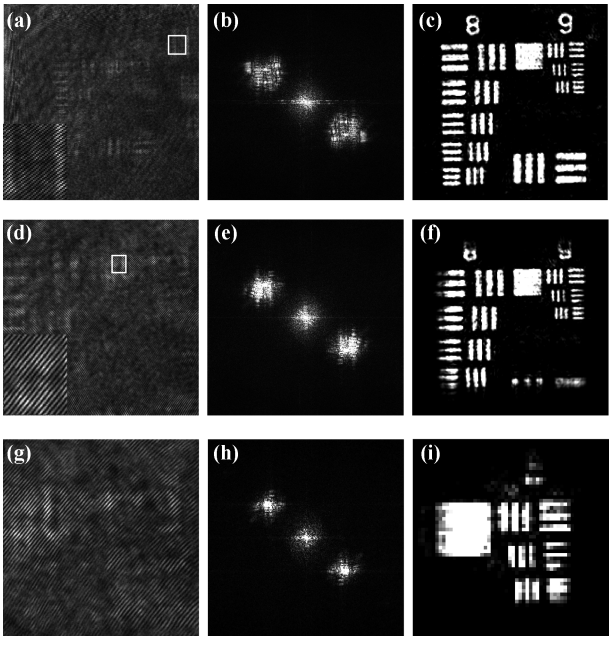

Fig. 8 The holograms (left columns) recorded by Post-MDHM, frequency spectral (middle columns) and reconstructed intensity images (right columns). **(a–c)** 1024×1024, **(d–f)** 512×512, **(g–i)** 256×256.

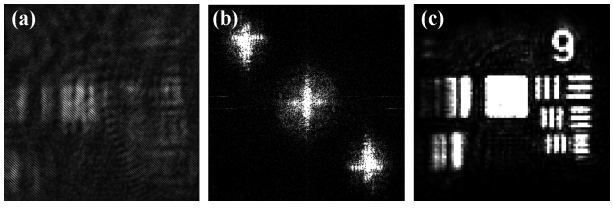

Fig. 9 The experimental results by Pre-MDHM. **(a)** hologram with 256×256, **(b)** frequency spectrum, and **(c)** reconstructed intensity images.

By comparing all the intensity images of Figs. 4 and 5 with Figs. 8 and 9, it is obvious that the lateral resolution and the image quality obtained by IPDHM is much better, especially when a CCD sensor with very small dimensions was used.

4 Conclusions

In conclusion, we have briefly derived the PSF of a practical regular Post-MDHM system with a finite-aperture MO and finite-dimension CCD sensor. The PSF of a regular practical IPDHM system, which takes into account the digitalization and pixel sampling effect, was also derived. The ULRs of these systems were analyzed and compared, and the results show that the imaging performance of Pre-MDHM is better than that of Post-MDHM in the same conditions. For the commonly used DHM, IPDHM is an optimal system, by which perfect imaging can be achieved. Except for simple numerical reconstruction and convenient selection of imaging area, IPDHM also possesses many other features, such as high resolution, high-quality imaging, and high accuracy of the phase image. In addition, the resolution has no correlation with the sensor dimensions and almost no relationship to the pixel size, which makes IPDHM more practical and easy to implement. High-resolution imaging close to the ULR of the used MO can be achieved by IPDHM even with a submillimeter-dimension sensor. Moreover, a special DHM with an infinity-corrected MO and a TL system in the object path performs better than the regular DHM.

Acknowledgements This work was supported by the National Natural Science Foundation of China (Grant Nos. 61077001, 61144005, and 61465005), the Natural Science Foundation of Hebei Province (Grant Nos. F2010001038, A2013402036, F2014402090, and A2015402035), the Technology Funding Project of Hebei Technology Office (Grant Nos. 09277101D and 13210201D), and the International Science and Technology Cooperation (Grant No. 2014DFE00200). The financial support of the four institutions is greatly acknowledged.

References

1. P. Picart and J. C. Li, Digital Holography, Wiley, Weinheim, 2013
2. D. Merrill, R. An, J. Turek, and D. D. Nolte, Digital holography of intracellular dynamics to probe tissue physiology, *Appl. Opt.* 54(1), A89 (2015)
3. Baxter, Digital holography: Counting cells, *Nat. Photonics* 5(9), 513 (2011)
4. M. Rinehart, H. Park, and A. Wax, Influence of defocus on quantitative analysis of microscopic objects and individual cells with digital holography, *Biomed. Opt. Express* 6(6), 2067 (2015)
5. L. Rong, T. Latychevskaia, C. Chen, D. Wang, Z. Yu, X. Zhou, Z. Li, H. Huang, Y. Wang, and Z. Zhou, Terahertz in-line digital holography of human hepatocellular carcinoma tissue, *Sci. Rep.* 5, 8445 (2015)
6. Y. Z. Zhang, D. Y. Wang, Y. X. Wang, and S. Q. Tao, Automatic compensation of total phase aberrations in digital holographic biological imaging, *Chin. Phys. Lett.* 28(11), 114209 (2011)
7. G. Di Caprio, A. El Mallahi, P. Ferraro, R. Dale, G. Coppola, B. Dale, G. Coppola, and F. Dubois, 4D tracking of clinical seminal samples for quantitative characterization of motility parameters, *Biomed. Opt. Express* 5(3), 690 (2014)
8. M. de Angelis, S. De Nicola, A. Finizio, G. Pierattini, P. Ferraro, S. Pelli, G. Righini, and S. Sebastiani, Digital-holography refractive-index-profile measurement of phase gratings, *Appl. Phys. Lett.* 88(11), 111114 (2006)
9. M. R. McCartney, D. J. Smith, R. Hull, J. C. Bean, E. Voelkl, and B. Frost, Direct observation of potential distribution across Si/Si p-n junctions using off-axis electron holography, *Appl. Phys. Lett.* 65(20), 2603 (1994)
10. C. Qin, J. Zhao, J. Di, L. Wang, Y. Yu, and W. Yuan, Visually testing the dynamic character of a blazed-angle adjustable grating by digital holographic microscopy, *Appl. Opt.* 48(5), 919 (2009)
11. T. Yanagawa, R. Abe, and Y. Hayasaki, Three-dimensional mapping of fluorescent nanoparticles using incoherent digital holography, *Opt. Lett.* 40(14), 3312 (2015)
12. S. Hosokawa, T. Ozaki, K. Hayashi, N. Happo, M. Fujiwara, K. Horii, P. Fons, A. V. Kolobov, and J. Tominaga, Existence of tetrahedral site symmetry about Ge atoms in a single-crystal film of $Ge_2Sb_2Te_5$ found by X-ray fluorescence holography, *Appl. Phys. Lett.* 90(13), 131913 (2007)
13. D. Pejchang, S. Coëtmellec, G. Gréhan, M. Brunel, D. Lebrun, A. Chaari, T. Grosges, and D. Barchiesi, Recovering the size of nanoparticles by digital in-line holography, *Opt. Express* 23(14), 18351 (2015)
14. K. Goto and Y. Hayasaki, Three-dimensional motion detection of a 20-nm gold nanoparticle using twilight-field digital holography with coherence regulation, *Opt. Lett.* 40(14), 3344 (2015)
15. J. Gao, D. R. Guildenbecher, L. Engvall, P. L. Reu, and J. Chen, Refinement of particle detection by the hybrid method in digital in-line holography, *Appl. Opt.* 53(27), G130 (2014)
16. N. Verrier, C. Fournier, and T. Fournel, 3D tracking the Brownian motion of colloidal particles using digital holographic microscopy and joint reconstruction, *Appl. Opt.* 54(16), 4996 (2015)
17. N. Verrier and C. Fournier, Digital holography super-resolution for accurate three-dimensional reconstruction of particle holograms, *Opt. Lett.* 40(2), 217 (2015)

18. A. L. Gaunt and Z. Hadzibabic, Robust digital holography for ultra-cold atom trapping, *Sci. Rep.* 2, 721 (2011)
19. S. L. Pu, Q. H. Wang, K. F. Cen, L. Denis, and K. F. Ren, Application of digital holography to circle flow bed boiler measurement, *Front. Energy* 1(2), 218 (2007)
20. P. Gao, G. Pedrini, and W. Osten, Phase retrieval with resolution enhancement by using structured illumination, *Opt. Lett.* 38(24), 5204 (2013)
21. P. Gao, G. Pedrini, C. Zuo, and W. Osten, Phase retrieval using spatially modulated illumination, *Opt. Lett.* 39(12), 3615 (2014)
22. D. Lee and A. Weiner, Optical phase imaging using a synthetic aperture phase retrieval technique, *Opt. Express* 22(8), 9380 (2014)
23. S. T. Thurman and A. Bratcher, Multiplexed synthetic-aperture digital holography, *Appl. Opt.* 54(3), 559 (2015)
24. C. J. Yuan, G. H. Situ, G. Pedrini, J. Ma, and W. Osten, Resolution improvement in digital holography by angular and polarization multiplexing, *Appl. Opt.* 50(7), B6 (2011)
25. M. Paturzo, F. Merola, S. Grilli, S. De Nicola, A. Finizio, and P. Ferraro, Super-resolution in digital holography by a two-dimensional dynamic phase grating, *Opt. Express* 16(21), 17107 (2008)
26. H. Wahba and T. Kreis, Characterization of graded index optical fibers by digital holographic interferometry, *Appl. Opt.* 48(8), 1573 (2009)
27. Y. C. Zhao, X. Y. Zhang, C. J. Yuan, S. P. Nie, Z. Q. Zhu, L. Wang, Y. Li, L. P. Gong, and S. T. Feng, Dark-field digital holographic microscopy by using vortex beam illumination, *Acta Physica Sinica* 63(22), 224202 (2014)
28. E. Sánchez-Ortiga, A. Doblas, G. Saavedra, M. Martínez-Corral, and J. Garcia Sucerquia, Off-axis digital holographic microscopy: practical design parameters for operating at diffraction limit, *Appl. Opt.* 53(10), 2058 (2014)
29. H. Y. Wang, M. J. Yu, Y. N. Jiang, Q. F. Zhu, and F. F. Liu, Point spread function and lateral resolution analysis of digital holographic microscopy system, *Opt. Commun.* 322, 90 (2014)